Attosecond Physics

Ferenc Krausz

Ludwig-Maximilians-Universität München, Max-Planck-Institut für Quantenoptik

D-85478 Garching, Germany, ferenc.krausz@mpq.mpg.de

An important class of motions in the microcosm takes place on a time scale of ~ 10^{-18} - 10^{-14} s and can be conveniently clocked in units of attoseconds (1 as = 10^{-18} s). It is the motion of electrons in atoms, molecules and nanoscale structures. The emission of visible, ultraviolet or x-ray light is a striking manifestation of attosecond-scale electron dynamics. Attosecond physics is the physics of electrons in motion at atomic and molecular length scales.

Electrons trigger or mediate virtually all processes in chemistry, biology and materials science. Insight into their motion in atoms, molecules and condensed matter would therefore impact many fields of science. The central goal of experimental attosecond physics is to develop tools and techniques for probing and controlling electronic dynamics in real time.

Control of the electromagnetic field of intense laser light has recently opened the door to attosecond metrology and spectroscopy. The reproducible generation and measurement of isolated 250-attosecond extreme ultraviolet pulses and first attosecond time-resolved observations of atomic electron dynamics indicate that experimental attosecond physics is coming of age.

Precision laser spectroscopy of antiprotonic helium atoms - weighing the antiproton to test the CPT invariance -

Ryugo S. Hayano[1]
Department of Physics, The University of Tokyo, 7-3-1 Bunkyo-ku, Tokyo, 113-0033, Japan

Although P (parity inversion), C (charge conjugation) and CP are known to be violated, simultaneous inversion of P, C and T (time reversal) is believed to keep physics laws unchanged (CPT theorem). In recent years, however, there are a number of string-motivated theories which accommodate CPT (as well as Lorentz symmetry) violations, making it important to experimentally test the CPT symmetry to the highest-possible precision. This can be done by comparing particle and antiparticle masses, or by comparing atom and anti-atom spectra.

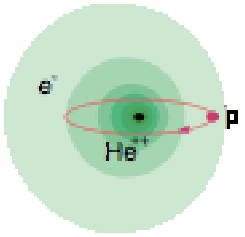

Fig. 1 Antiprotonic Helium

In 2002, we succeeded to produce a large number of antihydrogen (e^+ $\bar{p}$) atoms [1] at the antiproton decelerator facility at CERN (Geneva). By making enough of them in the ground state, we may be able to compare either the 1s-2s splitting or the ground-state hyperfine splitting of hydrogen vs antihydrogen to high precision; we have been working hard to achieve these goals, but there are still many hurdles to be cleared.

Meanwhile, we have made a significant progress in the precision spectroscopy of antiprotonic helium, with which we have measured the antiproton mass to better than 10^{-8} precision.

Antiprotonic helium (Fig. 1: $\bar{p}He^+$) is an exotic 3-body neutral system consisting of an antiproton, an electron and a helium nucleus. Usually, antiprotons cannot survive for longer than ~ps when injected into matter, but we serendipitously discovered that about 3% of antiprotons stopped in helium can survive for several microseconds. Subsequent studies established that the reason for this anomalous metastability is due to the formation of $\bar{p}He^+$ atom, in which the electron is in the ground orbit while the antiproton is in a highly-excited near-circular orbits (principal quantum number n~40, orbital quantum number L~40).

The importance of $\bar{p}He^+$ lies not just in its metastability, but in the fact that we can measure laser-resonant transitions between *(n,L)* and *(n-1, L-1)* antiproton orbits, and relate the transition frequency $\nu(n, n-1)$ to the antiproton mass (thereby "weighing" the antiproton). Our present published precision is $\delta m/m=10^{-8}$ [2], but by locking our laser system to a frequency comb, we have recently succeeded to reduce experimental errors by an order of magnitude. In a few years, we expect that the precision of antiproton mass measurement using $\bar{p}He^+$ will become as good as or even become better than the present proton mass precision of 0.46×10^{-9}.

[1]M. Amoretti et al., Nature **419**, 456 (2002)

[2]M. Hori *et al.*, Phys. Rev. Lett. **91**, 123401 (2003)

[1] hayano@phys.s.u-tokyo.ac.jp

Attosecond dynamics of electron wavepackets in intense laser fields

Katalin Varjú
Department of Physics, Lund Institute of Technology, P. O. Box 118, SE-221 00 Lund, Sweden
Katalin.Varju@fysik.lth.se

1. Generation and poscompression of attosecond pulse trains (APT)

In our experimental setup the APT is synthesized from the 13th to 35th harmonics of a 35 fs Ti:Sapphire laser. To achieve the required short on-target attosecond pulses, the harmonics are filtered spatially by an aperture and spectrally using variable thickness metallic filters. The metallic films also serve the purpose of compressing the attosecond pulses, that are chirped at generation [1], using their negative group-delay dispersion [2]. We are able to tailor the chirp and therefore duration of the attosecond pulses.

Part of the IR beam is split off before the generation to be used as the dressing pulse for the two color cross-correlation measurements. It goes through a variable delay line and is collinearly overlapped with the APT.

2. Generation and evolution of attosecond electron wavepackets in strong laser fields

Attosecond pulses interacting with a gas of atoms generate electron wavepackets (EWPs) which are temporally localized over approximately the same duration as the attosecond pulses and centered at an energy $W = hv_{xuv} - I_p$. Together with the fact that the pulses in an APT are naturally synchronized to the period of the driving field, this promises for a new range of experiments, where APTs are used as a controllable injection mechanism for EWPs in strong field experiments [3]. Fig. 1b. illustrates the effect of a strong infrared laser field on the EWP ejected at different phases of the IR beam. We observe the momentum transfer from the laser field to the EWP, which is strongly dependent on the relative delay of the two pulses. When the EWPs overlap with the zero crossings of the laser electric field – which corresponds to the maximum vector potential – we see the electron spectrum redistributed, and extending to higher energies than the original harmonic peaks by as much as 15 eV. When the EWPs overlap with the maximum of the laser electric fields, there is no momentum transfer from the laser field, but the pulses are being streaked by the rapidly varying vector potential. We also study the effect of the XUV chirp on the continuum dynamics, and present the results for a transform limited and a positively chirped EWP.

We obtain additional information on the momentum exchange between the EWP and of the IR laser field, by angularly resolving the electron spectrum, using a Velocity Map Imaging spectrometer [4]. We observe the momentum transfer from the laser field to the electron wavepacket, similar to that of [5], but this time with angular resolution [6] (See Fig. 1a). Additional to the previous work, taking advantage of the periodicity of the APT being twice that of the laser field, we also observe the interference of the two electron wavepackets, being launched at half period intervals, and therefore undergoing different momentum transfers. We compare the results to semiclassical calculations based on the Strong Field Appoximation, that provide an intuitive understanding of the dynamics, and to numerical results obtained from the Time Dependent Schrödinger Equation.

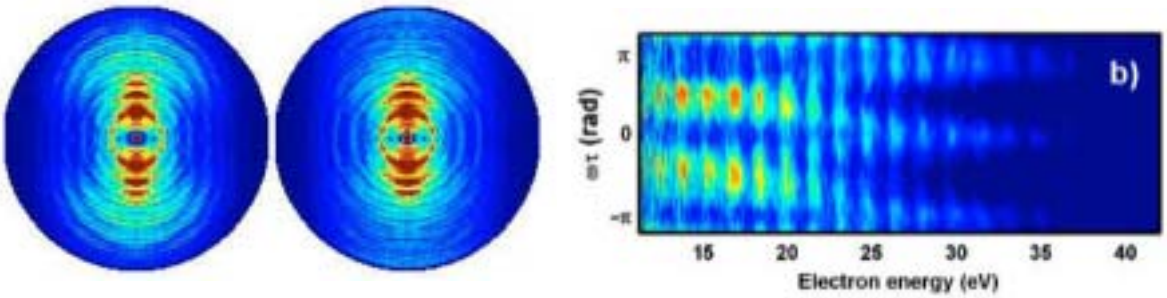

Fig. 1. a) Angularly resolved electron spectra at two delays between the XUV and IR pulses. b) Angularly integrated wo-colour photo-electron spectra with a train of 160 as pulses, and the IR field, as a function of delay.

4. References

[1] Y. Mairesse, *et al.*, "Attosecond Synchronization of High-Harmonic Soft X-rays" Science **302**, 1540-1543 (2003).
[2] R. López-Martens, *et al.*, "Amplitude and Phase Control of Attosecond Light Pulses," Phys. Rev. Lett. **94**, 033001 (2005).
[3] P. Johnsson, *et al.*, "Attosecond Electron Wave Packet Dynamics in Strong Laser Fields," Phys. Rev. Lett., **95**, 013001 (2005).
[4] S.A. Aseyev, *et al.*, "Attosecond Angle-Resolved Photoelectron Spectroscopy"Phys. Rev. Lett. **91**, 223902 (2003)
[5] E. Goulielmakis, *et al.*, "Direct Measurement of Light Waves", Science **305**, 1267-1269 (2004)
[6] T. Remetter, *et al.*, "Interference of Attosecond Electron Wavepackets", in preparation

Generation and Applications of Strong High Harmonics

Chang Hee Nam
Department of Physics and CXRC, KAIST, Yuseong-gu, Daejeon 305-701, Korea

High harmonic generation is a coherent interaction process between atoms and intense laser field and provides coherent soft x-ray radiation with ultrashort pulse duration. For applications of such harmonic light sources to ultrafast soft x-ray spectroscopy in the femtosecond and attosecond ranges and to soft x-ray interferometry/holography, the generation of bright high harmonics is very essential. Strong harmonic generation can be achieved by coherently driving a large number of atoms by intense laser pulses. We realized such conditions by obtaining self-guided and profile-flattened laser propagation in a long gas jet, allowing uniform phase matching of harmonics in a large volume [1], and we also coherently controlled high harmonic generation using chirped laser pulses to attain spectral sharpness of harmonics [2]. In addition, we recently achieved exceptionally strong harmonic generation in a two-color laser field consisted of the fundamental and second-harmonic of a high-power femtosecond laser [3]. Here, we present the methods of strong high harmonic generation and applications.

When intense femtosecond laser pulses propagate through an ionizing gas medium, the laser pulses are affected by modification of the refractive index of the medium and by plasma defocusing. The former alters the profile of the laser pulses in the time domain, while the latter in the space domain. To avoid the effects of the plasma defocusing, the conditions for self-guided and profile-flattened laser propagation have been investigated [4]. When the gas medium is placed before the laser focus, the plasma defocusing effect can be offset in the converging laser beam and the spatial profile of the laser beam is redistributed to a flattop intensity profile. The flattop laser profile also generates a flattened electron distribution, leading to a flattened refractive index profile with steep boundary. The flattened refractive index change at the boundary of flattened profile induces self-guided laser propagation. This self-guided and profile-flattened laser propagation is very favorable for bright harmonic generation because it ensures a nearly uniform laser field over a large volume.

On the other hand, the temporal modification of the laser pulses can be controlled by applying appropriately chirped laser pulses. The rapid ionization of gaseous medium by an intense laser pulse brings out the change of refractive index in time, which induces the self-phase modulation (SPM) of the laser pulse and develops a positive chirp in the leading edge of the laser pulse [5]. As the spectral structure of harmonics emitted is directly affected by the temporal structure of the laser pulse, the high harmonics exhibit a chirped structure. This chirped structure comes in part due to the rapid rising of the femtosecond laser pulse (intrinsic chirp) and due to the SPM-induced laser chirp. The chirped harmonic spectral structure is evidenced by broadened spectrum. In order for controlling the harmonic chirp, the temporal structure of the laser pulse can be tuned. As SPM induces a positive chirp to the laser pulse, it is found that a laser pulse with initial negative chirp is suitable for the compensation of the positive chirp, generating sharp harmonics.

Instead of driving atoms by single-color laser pulses, two-color laser pulses can be applied to atoms. By applying the fundamental and second harmonic fields of an intense

femtosecond laser pulse, efficient harmonic generation can be achieved. By combining laser pulses with different frequencies, various kinds of laser field can be synthesized so as to produce strong harmonics. Such parameters of the two-color fields as intensity, polarization, relative phase, and time delay between the two fields can be manipulated. When a two-color laser field suitable for strong harmonic generation is prepared, we may be able to achieve very efficient high harmonics.

First, experiments of strong high harmonic generation from neon using single-color femtosecond laser pulses are explained. Laser pulses of 27-fs duration and wavelength centered at 827 nm with 5-mJ energy were focused onto a long neon gas jet with a 9-mm slit nozzle. The self-guided propagation was accomplished by placing the gas jet at 18 mm before the laser focus. The spectral sharpness of the harmonics was optimized by applying a negatively chirped 42-fs laser pulse. With the application of self-guided and negatively chirped laser pulse, the efficiency of harmonics was very much enhanced and the divergence of harmonics was minimized. At the optimum conditions, the 61st harmonic at 13 nm has a divergence of 0.5 mrad and spectral bandwidth of 0.07 nm.

Next, efficient harmonic generation in a two-color laser field is discussed. By simply inserting a second harmonic crystal in the focused laser beam path and adjusting the relative phase between the fundamental and second harmonic components using a thin glass plate, we obtained extremely strong harmonics from neon in the 20 nm region. The harmonics generated with orthogonally polarized two-color field were much stronger than those generated in the two-color field with parallel polarization. We analyzed the results from the electron behavior in the two-color field.

Unique properties of harmonic x-ray sources are attractive for applications in ultrashort soft x-ray spectroscopy and soft x-ray interferometry. The harmonic x-ray sources are well suited for the investigations of atomic and molecular dynamics in the femtosecond and attosecond time scales, and also for the metrology of EUV optics by realizing a soft x-ray interferometry [6].

This work has been supported by the Korea Science and Engineering Foundation through the Creative Research Initiative Program.

References

[1] H. T. Kim, I J. Kim, D. G. Lee, K. H. Hong, Y. S. Lee, V. Tosa, and C. H. Nam, Phys. Rev. A **69**, 031805(R) (2004).
[2] D. G. Lee, J. H. Kim, K. H. Hong, and C. H. Nam, Phys. Rev. Lett. **87**, 243902 (2001).
[3] I J. Kim, C. M. Kim, H. T. Kim, G. H. Lee, Y. S. Lee, J,.Y. Park and C. H. Nam, Phys. Rev. Lett. **94,** 243901 (2005).
[4] V. Tosa, H.T. Kim, I.J. Kim, and C.H. Nam, Phys. Rev. A **71**, 063808 (2005).
[5] J. H. Kim and C. H. Nam, Phys. Rev. A **65**, 033801 (2002).
[6] D. G. Lee, J. J. Park, J. H. Sung, and C. H. Nam, Opt. Lett. **28**, 480 (2003).

High repetition rate tabletop soft x-ray lasers at wavelengths down to 13.2 nm

J.J. Rocca, B. M. Luther, Y. Wang, S. Heinbuch, M. A. Larotonda, D.Alessi,
M. Berrill, M.C. Marconi, C.S. Menoni, and V.N Shlyaptsev[1]
NSF ERC for Extreme Ultraviolet Science and Technology, , Colorado State University
[1] Department of Applied Science, University of California Davis-Livermore

Abstract: We discuss recent advances in high repetition rate soft x-ray lasers, which include the demonstration of 5Hz repetition rate table-top soft x-ray lasers producing microwatt average powers at wavelengths ranging from 13.2 to 32.6 nm. The results were obtained by collisional electron excitation of Ni-like and Ne-like ions in plasmas efficiently heated with picosecond optical laser pulses of only 1 J energy impinging at grazing incidence. The operation of an extremely compact desk-top size 46.9 nm capillary discharge laser at repetition rates up to 12 Hz with 0.15 mW average power is also reported.

There is significant interest in the development of table-top sources of high average power soft x-ray radiation for applications. In the past several years gain-saturated soft x-ray laser operation at wavelengths above 30 nm was demonstrated at repetition rates up to 10 Hz using fast discharge excitation of capillary plasmas [1] as well as optical field ionization [2]. Gain-saturated operation has been also obtained at repetition rates of one shot every several minutes for wavelengths as low as 13.9 nm by transient collisional electron excitation of targets with 3-10 J of short pulse laser pump energy impinging at normal incidence [3-5]. Several experiments have observed lasing at 18.9 nm in Ni-like Mo using small pump energies [6-8]. Recently, it has been demonstrated that the pumping efficiency of collisionaly excited soft x-ray lasers can be significantly increased by directing the short pulse at grazing incidence [9-12]. This

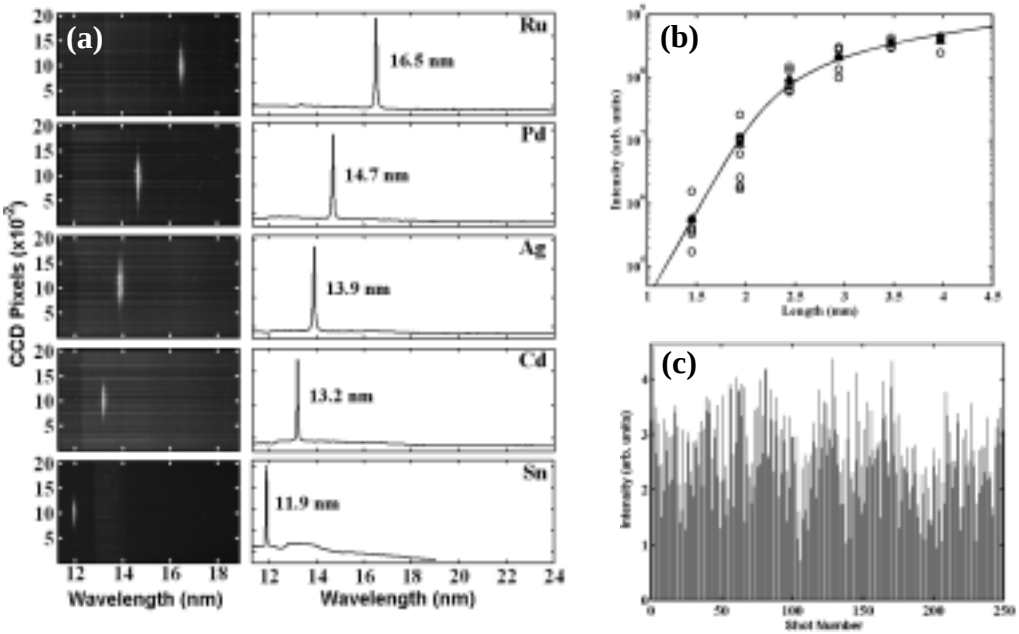

Fig. 1. – (a) Single shot on-axis spectra of 4 mm line focus plasmas showing lasing in the $4d^1S_0$- $4p^1P_1$ transition of the Ni-like ions at wavelengths ranging from 16.5 to 11.9nm. (b) Intensity versus target length for the 13.9nm line of Ni-like Ag showing a small signal gain of 67.5cm^{-1} and a gain-length product of $g \times l$=16.8. (c) Shot-to-shot variation of the intensity of the 13.9nm Ni-like Ag laser line at 5Hz repetition rate.

pumping geometry takes advantage of refraction of the pump beam in the plasma to increase the path length in the gain region and the absorption efficiency of the pump energy in that region.

Hence a large fraction of the pump energy (typically 20 to 50 percent) can be selectively deposited into the gain region. We have demonstrated 5 Hz repetition rate operation of gain-saturated table-top lasers in transitions of Ni-like ions (Mo, Ru, Pd, Ag and Cd- see Fig 1a) and Ne-like (Ti and V) ions at wavelengths of 18.9, 16.5, 14,7, 13.9, 13.2 nm, and 32.6 and 30.4 nm respectively. Soft x-ray laser average powers of 1-2 microwatt were obtained using an 8 ps heating pulse with an energy of ~1 J from a Ti:sa laser impinging at grazing angles between 17 and 23 degrees. Strong amplification was also observed at 11.9 nm in Ni-like Sn. Figure 1(a) shows on-axis spectra corresponding to 4 mm long plasmas of, Ru (Z = 44), Pd (Z = 46), Ag (Z = 47), Cd (Z =48), and Sn (Z=50) irradiated at a grazing incidence angle of 20 degrees. Figure 1(b) shows the results of gain measurements for the 13.9 nm line of Ni-like Ag. The intensity is observed to increase rapidly as a function of target length with a gain coefficient of 67.5 cm^{-1}, until it rolls off into saturation to reach a gain-length product of $g \times l$ =16.8. Similar gain-length products were measured for Mo, Ru, Pd and Cd. Figure 1(c) illustrates 5 Hz repetition rate operation of the Ni-like Ag laser for 250 contiguous shots. The energy of the most intense shots 800 nJ and the average power approaches 2 μW. Saturated laser operation at 5 Hz repetition rate with gain-length products of about 20 was also obtained for transition of Ne-like Ti and V with wavelength near 30 nm [11], with resulting average powers of about 1.5 to 2.5 μW.

In a separate development, the first of a new generation of desk-top size capillary discharge lasers was demonstrated to generate an average power of 0.15 mW in the 46.9 nm line of Ne-like Ar using a capillary discharge set up that is significantly more compact than its predecessors and that does not require a Marx generator. It is to our knowledge the first soft x-ray laser to fit onto a small desk and to be easily transportable It emits 13 μJ pulses of λ= 46.9 nm light at 12 Hz repetition rate, corresponding to an average power of ~ 0.15 mW. The laser occupies a table area of about 0.4 × 0.4 m^2. The reduced size of this capillary discharge device is achieved making use of a very low inductance co-axial discharge configuration [13] that decreases the voltage necessary to generate the peak current required for laser excitation to < 90 kV. As a result the volume of the pulsed power unit is ~ 9 times smaller than that of previous capillary discharge lasers [1]. Capillary lifetime tests at 12 Hz repetition rate show the laser output energy decays by 2X after about 2 10^4- 3 10^4 shots. This laser is currently routinely used as a single photon ionization source in a nanocluster mass spectroscopy experiment.

Conclusion: High repetition rate operation of gain-saturated lasers was demonstrated at several wavelengths between 13.2 and 46.9 nm in transitions of Ni-like and Ne-like ions. It will be possible to use these lasers for high resolution imaging, interferometry, and other applications.

Work was supported by the NSF ERC for Extreme Ultraviolet Science and Technology, NSF Award EEC-0310717

References

1. B. R. Benware, C. Macchieto, C. Moreno, J. J. Rocca, Phys. Rev. Lett. **81**. 5804 (1998), and C. D. Macchieto, et al. Opt. Lett. **24** 1115 (1999)
2. S. Sebban,. R. Haroutunian, Ph. Balcou, *et al*, Phys. Rev. Lett. **86**, 3004, (2001) and S. Sebban, et al. Phys. Rev. Lett. **89**, 253901 (2002)
3. P.V. Nickles, V.N. Shyapstev, M. Kalachinkov, M. Schnuer, Phys. Rev. Lett. **78,** 2748 (1997)
4. J. Dunn, Y. Li, A. L. Osterheld, J. Nilsen, J. R. Hunter, V. N. Shlyaptsev, Phys. Rev. Lett. **84**, 4834 (2000)
5. K.A. Jenulewicz, A. Lucianetti, G. Pruebe, W. Sadner and P.V. Nickles. Phys. Rev. A **68,** 051802, (2003)
6. T. Ozaki, R. A. Ganeev, A. Ishizawa, T. Kanai, H. Kuroda, Phys. Rev. Lett. **89,** 253902 (2002),
7. R. Li and Z. Z. Xu Journal de Physique IV, **11** (PR2) 27 (2001)
8. R. Tommasini, J. Nilsen, E. E. Fill, Proc. of SPIE **4505**, 85 (2001)
9. R. Keenan, J. Dunn, P. K. Patel, D. F. Price, R. F. Smith, V. N. Shlyaptsev, Phys. Rev. Lett. , **94**, 103901, (2005)
10. B. M. Luther, Y. Wang, M. Larotonda, D. Alessi, M. Berrill, M. Marconi, V. Shlyaptsev, J. J. Rocca, Optics Lett., **30**, 165, (2005)
11. D. Alessi, B. M. Luther, Y. Wang, M. A. Larotonda, M. Berrill, J. J. Rocca, *Opt. Express,*. **13**,. 2093, (2005).
12. Y. Wang, M. A. Larotonda, B. M. Luther, M. C. Marconi, D. Alessi, M. Berrill, V. N. Shlyaptsev, and J. J. Rocca, "Demonstration of saturated high repetition rate tabletop soft x-ray lasers at wavelengths down to 13.9 nm", in press *Phys. Rev. A.*
13. S. Heinbuch , M. Grisham, D. Martz and J.J. Rocca. Optics Express, **13**, 4050, (2005

Octave Spanning Ti:sapphire Lasers

F. X. Kärtner
Department of Electrical Engineering and Computer Science, and Research Laboratory of Electronics, Massachusetts Institute of Technology, 77 Massachusetts Avenue, Cambridge, MA 02139, USA

Abstract: Generation of femtosecond laser frequency combs and carrier- envelope phase stabilized ultrashort pulses with less than 7fs in duration directly from octave-spanning Ti:sapphire lasers is demonstrated.

Summary:
Femtosecond laser based optical frequency combs have revolutionized optical frequency metrology [1,2]. This revolution was driven by recent developments in solid-state lasers providing trains of low jitter ultrashort laser pulses. Specifically, high-repetition rate Ti:sapphire laser based frequency combs still provide the highest quality frequency combs enabling the construction of clock works with the highest stability. In the time domain, carrier envelope phase stabilized high energy pulses enabled the generation of isolated attosecond pulses [3]. Here, we report on our progress in constructing octave spanning Ti:sapphire lasers that can be directly self-referenced using f-to-2f interferometry.

The complete experimental setup is depicted in Fig. 1. The Ti:sapphire laser is similar to the one described in Ref. [5]. It employs double-chirped mirror pairs and a BaF2-plate and wedges for precise dispersion control and repetition rate scaling.

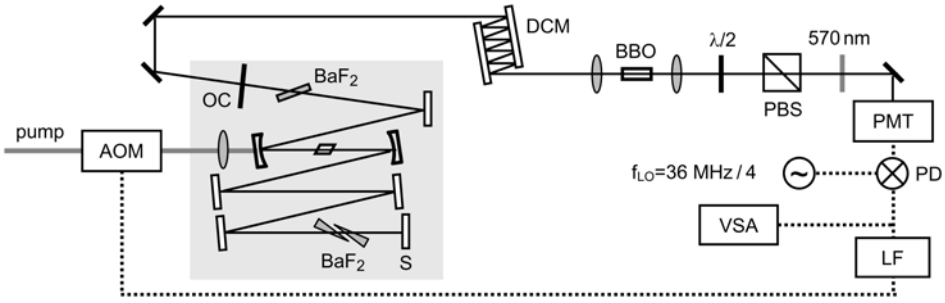

Figure 1: Carrier-envelope phase stabilized 200 MHz octave-spanning Ti:sapphire laser. The femtosecond laser itself is located inside the grey area. AOM, acousto-optical modulator; S, silver end mirror; OC, ouput coupling mirror; PBS, polarizing beam splitter cube; PMT, photomultiplier tube; PD, digital phase detector; LF, loop filter; VSA, vector signal analyzer. The carrier-envelope frequency is phase locked to 170 MHz.

.Afterwards, the Ti:sapphire output is focused into a 2 mm thick BBO crystal cut for type I second-harmonic generation (SHG) of 1160 nm. The generated SHG light and the orthogonally polarized fundamental light are projected onto a common polarization axis using a half-waveplate and a polarizing beam splitter cube. After spectral prefiltering the interference beat is detected using a photomultiplier tube (Hamamatsu H6780-20). The measured radio-frequency power spectrum shows a carrier-envelope frequency beat signal with a SNR of ~35 dB in a 100 kHz resolution bandwidth, sufficient for direct carrier-envelope phase stabilization. The femtosecond laser is pumped by ~6 W of 532 nm light from a frequency-doubled Nd:YVO4 pump laser. The total output power of the laser is about 250 mW. Behind a 10 nm interference filter centered at 570 nm and 1140 nm power levels of ~1 μW and ~1 mW have been measured. The time delay between those two

wavelengths used for self-referencing is adjusted using a chirped mirror delay line.

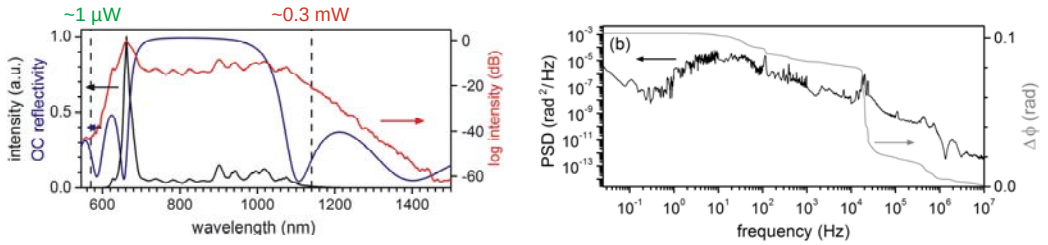

Figure 2: (a) Output spectrum of the Ti:sapphire laser on a linear (black curve) and on a logarithmic scale (red curve); reflectivity of the output coupler (blue curve). The wavelengths 570 and 1140 nm used for self-referencing are indicated by two dashed lines. (b) carrier-envelope phase noise power spectral density (left) and integrated phase jitter (right) resulting in only 45 as accumulated carrier-envelope timing jitter.

Phase locking is achieved by feeding the error signal from the digital phase detector to an AOM placed in the pump beam (see Fig. 1) which modulates the pump power and thus changes the carrier-envelope frequency. Fig. 2(b) shows the power spectral density (PSD) of the carrier-envelope phase fluctuations. The integrated phase error from 1mHz to 10MHz is only 0.10 rad corresponding to 45 as carrier-envelope timing jitter, which can be further improved in the future by using an EOM in the feedback loop.

Similar results can be obtained for the carrier-envelope phase error , if the ouput pulse is reflected off from the same output coupler as shown in Fig. 2a and only the transmitted spectral components at 1140 and 570 nm are used for the carrier-envelope phase lock. The reflected pulse shows a width of less than 7fs, when characterized with an interferometric autocorrelator and reconstructed using the PICASSO algorithm. Further pulse reduction is possible by suppressing the spectral spike at 670 nm caused by the finite bandwidth of the output coupler. Using prism based pulse shapers, pulses as short as 4.3 fs have been generated directly form octave spanning Ti:sapphire lasers [5].

References

1. T. Udem, J. Reichert, R. Holzwarth, T. W. Hänsch, Phys. Rev. Lett. **82**, 3568 (1999).
2. D. J. Jones, S. A. Diddams, J. K. Ranka, R. S. Windeler, J. L. Hall, S. T. Cundiff, Science 288, 635 (2000).
3. M. Hentschel, R. Kienberger, Ch. Spielmann, G. A. Reider, N. Milosevic, T. Brabec, P. Corkum, U. Heinzmann, M. Drescher and F. Krausz, Nature 414, 509-513 (2001).
4. L. Matos, D. Kleppner, O. Kuzucu, T. R. Schibli, J. Kim, E. P. Ippen, and F. X. Kaertner, Opt. Lett. 29, 1683 (2004).
5. T. Binhammer, E. Rittweger, R. Ell, F.X. Kärtner, and U. Morgner, “Novel prism-based pulse shaper for octave spanning spectra,” to appear in IEEE J. of Quant. Electronics.

Stabilization and control of carrier-envelope phase and instantaneous structure resolved by real-time spectroscopy

Takayoshi Kobayashi Shunsuke Adachi, and Xiaojun Fang and Yoshiharu Yuasa
Department of physics, Graduate School of Science, University of Tokyo, 7-3-1 Hongo, Bunkyo-ku, Tokyo, 113-0033, Japan
Tel. +81-3-5841-4228, Fax. +81-3-5841-4240, yuasa@femto.phys.s.u-tokyo.ac.jp

In this talk I would like to talk on the following two subjects. The first one is on the phase of extremely short pulses and the second one is on the molecular coherent vibration impulsively excited by an ultrashort pulses.

I. Carrier-phase envelope(CEP) stabilization and CEP dependent photochemistry

Self-stabilization was verified for the carrier-envelope phase of idler pulses from a noncollinear optical parametric amplifier (NOPA)[1,2] by spectral interference[3] between supercontinuum (SC) and its second harmonic. SC is obtained by transmission of the idler through a photonic-crystal fiber. Compressed idler pulse from NOPA with a deformable mirror was characterized by SFM XFROG and long-term CEP of the idler was stabilized and controlled by *f*-to-2*f* interferometry scheme shown in Fig. 1.

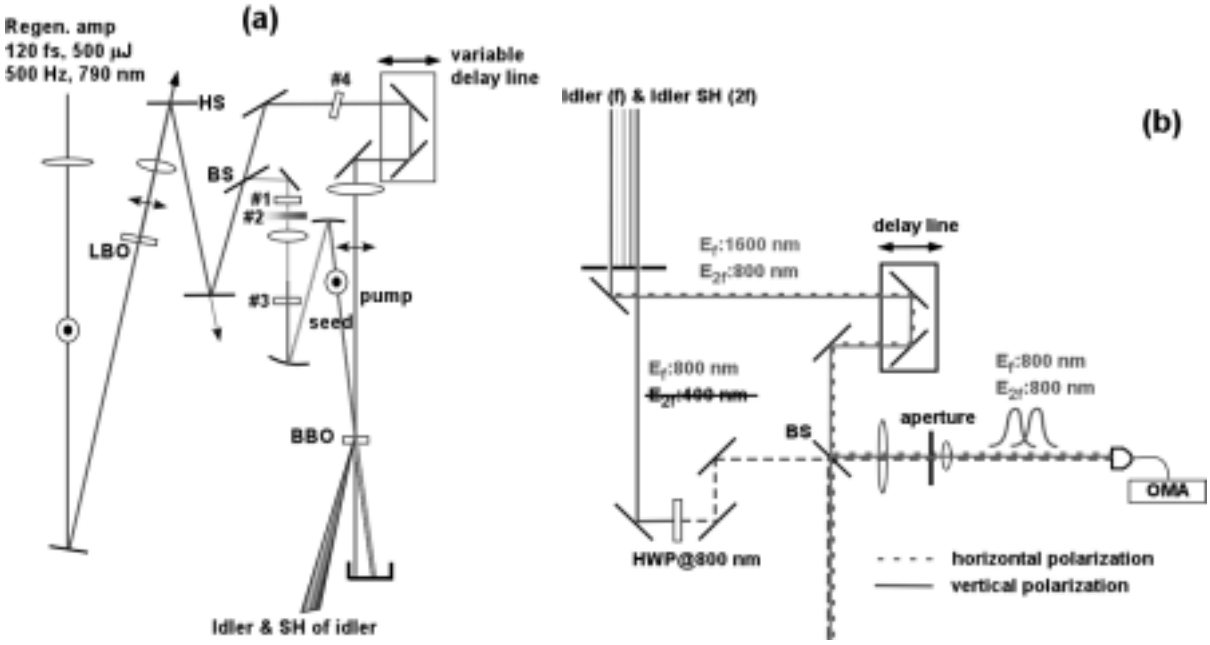

Fig.1. (a)Setup of CEP self-stabilizing NOPA. #1: λ/2 wave plate; #2: variable neutral density filter; #3: 2-mm-thick CaF_2 plate on vertical rotation stage to avoid damages due to high peak pulse energies; #4: 1-mm-thick CaF_2 plate on horizontal rotation stage for CEP stabilization and control of the idler output. (b)Setup of *f*-to-2*f* interferometry for the CEP drift measurement.

II. Real-time molecular vibrational frequency and amplitude probing to resolve instantaneous structure

Optical and electrical properties of conjugated polymers have attracted enormous attention because of their unique properties as model compounds of one-dimensional electronic systems.

Among conjugated polymers polydiacetylenes (PDA's) have special interests because of their large nonlinearity. The ultrafast optical responses in PDA's have been intensively investigated using femtosecond absorption spectroscopy. The mechanism was explained by the following model. First, photoexcited ^1B_u free exciton (FE) relaxes to the nonfluorescent ^1A_g state, which lies lower than the ^1B_u exciton. The nonthermal ^1A_g state relaxes to the bottom of potential curve of the self-trapped exciton (STE) state and then thermalizes and then relaxes to the ground state.

In the present paper, real time evolution of the energies and intensities of features in transmittance change spectra was investigated and real-time vibrational frequencies of several modes were found to provide important information of instantaneous structure of polymers.

In the normalized difference transmission ($\Delta T/T$) spectra, two components with different lifetimes were separated by the singular value decomposition (SVD) method. One is short-lived component of about 60 fs and the other is long-lived component of about 0.9 ps. In the separated spectrum of short-lived component, five positive peaks are found which are assigned to induced emission from the excited-state (ES) vibrational levels to the ground-state (GS) vibrational levels where no population exists because of much larger energies of the levels than the thermal energy of these peaks. Negative peaks in short-lived components could be due to induced absorption, but probe photon energy measured in this study is out of the range of two-photon absorption peaks from the ground state. Therefore only one-photon absorption is to be taken into account in the energy region from 1.68 to 2.28 eV and no induced absorption from 1^1B_u is appeared in short-lived component.

The transition energy from ES to GS is directly observed and it is found to shift to lower energy associated with the decay process from 1^1B_u FE to STE and geometrically relaxed 2^1A_g state after photo-excitation. The time constant of the Stokes shift agrees well with decay time (~60 fs) of the induced emission. This is quite reasonable if we consider the facts that the quantum efficiency of emission is smaller than 10^{-5}. Stokes shift has been estimated to be about 90 meV in PDA-3BCMU and 100 meV in red phase of PDA-4BCMU by stationary fluorescence spectra. The binding energy of the STE in red-phase 3BCMU is smaller than that of blue-phase 3BCMU as known from the fact that zero phonon transition energy in the former is larger than that of the latter. Therefore, the configuration in the excited state of 4BCMU is considered to be unstable and hence Stokes shift is larger than in 3BCMU.

The time trace of a short-lived peak near 1.88 eV, which disappear within 100 fs, is shown to be modulated in both its intensity and transition energy by molecular vibration of which oscillation period is being up-chirped from that of C-C double-bond stretching to that of triple-bond stretching. This clearly indicates that the molecular geometrical relaxation takes place from acetylene-type to butatriene-type within 10fs and relax back to the acetylene-type configuration within 100fs.

References

[1] A. Shirakawa, I. Sakane, and T. Kobayashi, “Pulse-front-matched optical parametric amplification for sub-10-fs pulse generation tunable in the visible and near infrared,” Opt. Lett. **23**, 1292 (1998)

[2] A. Baltuška, T. Fuji, and T. Kobayashi, “ Visible pulse compression to 4 fs by optical parametric amplification and programmable dispersion control,” Opt. Lett. **27**, 306 (2002)

[3] A. Baltuška, T. Fuji, and T. Kobayashi, “Controlling the carrier-envelop phase of ultrashort light pulses with optical parametric amplifiers,” Phys. Rev. Lett. **88**, 133901 (2002)

Ultrafast, Nonlinear, and Active Nanoplasmonics

Mark I. Stockman
Department of Physics and Astronomy, Georgia State University, Atlanta, GA 30303, USA
E-mail: mstockman@gsu.edu, web page: http://www.phy-astr.gsu.edu/stockman

1. Introduction

We consider the latest developments in ultrafast, nonlinear (including strong-field) nanoplasmonics, i.e., physics of optical fields localized at the nanoscale whose spatio-temporal dynamics is mediated by surface plasmon polaritons (SPPs) and surface plasmons (SPs). While the free-propagating and guided electromagnetic waves cannot be localized to a region significantly smaller than the wavelength, the plasmonic waves can and do nanolocalize [1-10]. We consider both the fundamentals, including some examples and illustrations, related experiments, and possible applications.

Special attention will be devoted to ultrafast nonlinear photoprocesses. The phenomena that are nanoscale and ultrafast have recently attracted significant attention, most of which are devoted to interaction of ultrashort laser pulses with metal nanostructures.

2. Coherent control of ultrafast energy localization on nanoscale

There exists a formidable problem of the control of nanoscale localization of optical energy. A characteristic wavelength of the optical radiation is orders of magnitude larger that the nanometer-scale distances at which the control is needed. In other words, light is devoid of the spatial degrees of freedom on the nanoscale. Therefore, one cannot produce a focusing of light on a nanoscale spot, except with adiabatic couplers [9], which can only be static.

We have shown that using the ideas of coherent control, one can achieve spatio-temporal control on the nanometer spatial scale and femtosecond temporal scale in metal nanostructures [2, 8]. The phase degrees of freedom of a light waveform are effective in controlling spatio-temporal kinetics of local optical fields. For nonlinear processes, the integral output is coherently controllable.

These predictions have been recently confirmed in direct experiments where two-pulse coherent control of two-photon electron emission by nanostructures has been observed in an experiment by H. Petek's group [11]. The excitation of a nanostructured system (a rough silver surface) was done with pairs 3.0 eV uv pulses of several fs duration; the interval τ between the pulses in a pair was controllable with ~ 100 as time steps. The electron emission was spatially resolved on the nanoscale using electron microscope. Note that energy of a photon is below the workfunction, so the entire photoemission is a two-photon process. These experiments has observed a nanoscale pattern of electron-emission hot spots that strongly depends on τ. We present the corresponding theory.

Apart from the two-photon emission mechanism, we also consider a strong, quasistationary field emission that occurs at a relatively low values of the Keldysh parameter. In this case, the dependence of the electron photoemission on parameters of the radiation becomes exponentially strong, and correspondingly the coherent control becomes very efficient. In this quasistationary case, a pair of ultrashort pulses at a given delay between pulses excites, in a typical case, a single emission hot spot. When this delay is changed, the emission hot spot jumps to a new position.

3. Surface plasmon amplification by stimulated emission of radiation (spaser)

We make a step towards quantum nanoplasmonics: surface plasmon fields of a nanosystem are quantized and their stimulated emission is considered. We introduce SPASER, a quantum generator for surface plasmon quanta. Spaser is predicted to generate ultrafast (10 to 100 fs

duration), temporally coherent, near-atomic intensity fields of surface plasmon modes that are strongly localized on the nanoscale. Those include dark modes that may constitute a basis for background-free enhanced nano-optical spectroscopy. Applications and related phenomena are discussed [3].

We have proposed to excite local fields using surface plasmon amplification by stimulated emission of radiation (spaser) [3]. The spaser radiation consists of SPs that are bosons and undergo stimulated emission, but in contrast to photons can be localized on the nanoscale. Spaser as a system will incorporate an active medium formed by two-level emitters, excited in the same way as a laser active medium: optically, or electrically, or chemically, etc. One promising type of such emitters are quantum dots (QDs). These emitters transfer their excitation energy by radiationless transitions to a resonant nanosystem that plays the role of a laser cavity. Spaser generates temporarily coherent local optical fields of almost atomic strength. It is predicted to be an ultrafast device.

Recently, the spaser effect has been observed in a proof-of principle experiment by L. Eng and collaborators [12]. In this experiment, the stimulated emission of SPs has been observed by a enhanced reflection of light from a metal surface due to the spaser effect partially compensating for losses in the metal.

4. Concluding discussion

Nanoplasmonics, i.e., a branch of nanooptics dealing with nanoscale localization of optical energy in metal nanostructures, is known for greatly enhanced optical effects induced by the nanoscale local optical fields. In this talk, we show that the nanoplasmonics is also an emerging direction of ultrafast and ultrastrong field science. Interest in nanoplasmonic systems is due to both their unique, reach fundamental physics and many existing and prospective applications. Among those application we can emphasize ultrafast control of the nanoscale electronics that can be achieved using the ideas of the coherent control on nanoscale that we proposed. The spaser, when implemented as a quantum generator will over wide opportunities as a ultrafast source of superstrong, nanoscale localized fields.

5. References

[1]. M. I. Stockman, S. V. Faleev, and D. J. Bergman, Phys. Rev. Lett. **87**, 167401 (2001).

[2]. M. I. Stockman, S. V. Faleev, and D. J. Bergman, Phys. Rev. Lett. **88**, 67402 (2002).

[3]. D. J. Bergman and M. I. Stockman, Phys. Rev. Lett. **90**, 027402 (2003).

[4]. K. Li, M. I. Stockman, and D. J. Bergman, Phys. Rev. Lett. **91**, 227402 (2003).

[5]. A. A. Mikhailovsky, M. A. Petruska, M. I. Stockman, et al., Opt. Lett. **28**, 1686 (2003).

[6]. I. A. Larkin, M. I. Stockman, M. Achermann, et al., Phys. Rev. B **69**, 121403(R) (2004).

[7]. M. I. Stockman, D. J. Bergman, C. Anceau, et al., Phys. Rev. Lett. **92**, 057402 (2004).

[8]. M. I. Stockman, D. J. Bergman, and T. Kobayashi, Phys. Rev. B **69**, 054202 (2004).

[9]. M. I. Stockman, Phys. Rev. Lett. **93**, 137404 (2004).

[10]. I. A. Larkin and M. I. Stockman, Nano Lett. **5**, 339 (2005).

[11]. A. Kubo, K. Onda, H. Petek, et al., Nano Lett. **5**, 1123 (2005).

[12]. J. Seidel, S. Grafstroem, and L. Eng, Phys. Rev. Lett. **94**, 177401 (2005).

Studies of Advanced Soft X-ray lasers and High Harmonic Generation

Hiroto Kuroda, Rashid Ganeev*, Masayuki Suzuki, Motoyoshi Baba,
Jun Zhang, He Xingui, and Jia Tianging, and
Institute for Solid State Physics, The University of Tokyo, 5-1-5 Kashiwanoha, Kashiwa-shi, Chiba, 277-8581, Japan
Tsuneyuki Ozaki
Institut national de la recherche scientifique, 1650 boul. Lionel-Boulet Varennes (Quebec) Canada J3X 1S2

The laser plasma has long been used as a medium for harmonic generation. The high-order harmonic generation (HHG) in visible and extreme ultraviolet (XUV) ranges has been investigated in the laser plasma formed by optical breakdown in gases and at the surface of solid targets (see [1] and references therein). However, the maximum observed order of harmonics reported in those studies was limited to the 27^{th} one due to some concurred effects in high-excited plasma. No plateau pattern for high harmonics was reported in those studies.

We demonstrate the generation of up to the 63^{rd} harmonic (12.6 nm) of a Ti: sapphire laser pulse (150 fs, 10 mJ), using prepulse (210 ps, 24 mJ) produced boron plasma as the nonlinear medium. The influence of various parameters on the harmonic conversion efficiency was analyzed. The steep decrease of the intensity for low-order harmonics (up to 19^{th} order) was followed by a plateau [1]. Typical conversion efficiencies were evaluated to be between 10^{-4} (for third harmonic) and 10^{-7} (within the plateau region). Harmonic generation appeared to be efficient in the case of the plasma consisted on neutral atoms and singly ionized boron. Typical divergence was found as small as 0.2 mrad. The strong harmonic radiation (61.2 nm) with output intensity almost 60 times higher than neighbor harmonics and conversion efficiency of $6x10^{-5}$ was observed. The main contribution to the limitation of harmonic generation efficiency and cutoff energy was caused by the self-defocusing of main beam. Spectral measurements showed that the high conversion efficiency of 13^{th} harmonic was caused by resonance enhancement of nonlinear susceptibility of indium plasma in the vicinity of 61 nm. So far, we have demonstrated new scheme of 18.9 nm soft x-ray laser in Mo plasma [2]. Present status of our activities on coherent soft x-ray light source will be reviewed.

Reference

[1] R. A. Ganeev, M. Suzuki, M. Baba, H. Kuroda, and T. Ozaki, Opt. Lett. **30**, 768 (2005).

[2] T. Ozaki, R. A. Ganeev, H. Kuroda, *et al*., Phys. Rev. Lett. **89**, 253902 (2002).

*Present address: NPO Akademgorodok, Tashkent 700125, Uzbekistan

Soft X-ray lasers seeded by a high harmonic beam

S. Sebban[a], Ph. Zeitoun[a], G. Faivre[a], T. Mocek[b], M. Fajardo[c], S. Kazamias[d], B. Cros [e],. G. Vieux [e] and G. Maynard [d]

[a] LOA, 91128 Palaiseau, France
[b] Institute of Physics, Department of X-Ray Lasers, Prague, Czech Republic
[c] GoLP, Instituto Superior Technico, Lisbon, Portugal
[d] LIXAM, bât. 350, Université Paris-Sud, 91405 Orsay, France
[e] LPGP, Université Paris-Sud, 91405 Orsay, France
stephane.sebban@ensta.fr

Since some years x-ray laser community try to promote this source for applications. In this aim, it is necessary to offer an optically good beam to the users. Nevertheless most of x-ray lasers (XRL) are using amplified spontaneous emission, i. e. laser has no cavity to select a spatial mode. Consequently the beam can not be polarized or spatially coherent and the wave front is not regular. Thanks to the most recent works on x-ray laser and on high order harmonics (HHG), it is now possible to produce an energetic beam (from 0.1 to 1mJ) having at the same time the required optical properties. The solution consists in seeding the XRL amplifier medium with another beam (HHG). This experiment was successfully realized in LOA. We studied seeding of two x-ray laser transitions, 32.8 nm (Kr^{8+}) and 41.8 nm (Xe^{8+}). We succeeded to increase from a factor 10 to 200 the HHG energy, without damaging their optical qualities [1]. The resulting beam was polarized, coherent. This geometry permits considerable improvements compare to the non-seeded XRL. Furthermore this technique can help for the measurement of many plasma parameters.

The XUV amplifying laser chain was made of three parts: a high harmonics generation (HHG) seed, a focusing system, and an optical field ionized x-ray laser (XRL) amplifier medium. The seed beam was obtained by focusing a 20 mJ, 30 fs, infrared laser in a gas cell filled with argon or xenon [2].This seed was image relayed onto the entrance of the x-ray laser (XRL) amplifier (Kr or Xe gas longitudinally pumped by a 1 J, 30 fs laser) by means of a toroidal XUV mirror. This X-ray laser operates at 32.8 nm and 42.8 nm using Kr and Xe respectively [3-5]. After amplification, the output beam was either analyzed by an XUV spectrometer or XUV CCD camera.

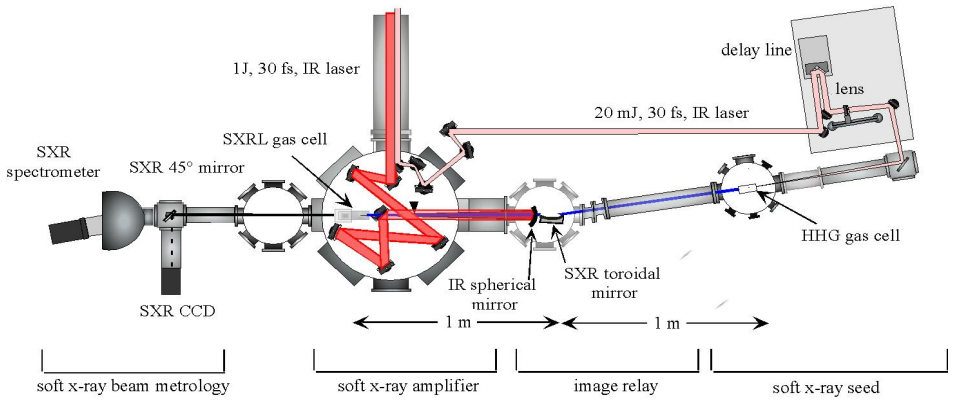

Figure 1 : Schematic description of the experimental set-up

The delay between XRL plasma creation and HHG injection was variable to reach optimum amplification conditions, synchronizing HHG seeding with maximum gain. Four emission spectra are displayed in figure 2, corresponding to (a) high harmonics alone, (b) x-ray laser alone, (c) XRL and HHG seeded long after gain extinction, and (d) HHG synchronised with maximum XRL gain. The amplification period starts 5 ps after the interaction of the IR laser with the gas and lasts about 8 ps. Figure 2 (d) clearly shows that a

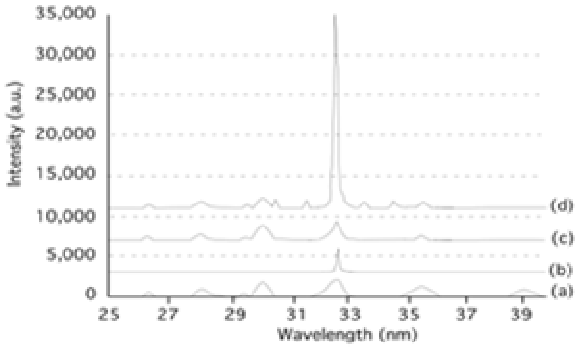

Figure 2 : Experimental spectra under conditions : (a) HHG only, (b) ASE XRL only, (c) both HHG and XRL in a non-amplifying timing, and (d) the amplified seeded XRL.

strong amplification of the seed has been achieved. The HHG were seeded at about twice the intensity of the ASE x-ray laser, leading to an enhancement of the output signal by a factor of 13. Since the level of seeding may influence many laser parameters (intensity, pulse duration, ratio of the energies in the seeded beam to this in the ASE beam), it is crucial to understand how is the seeding level related to the saturation intensity.

The seeded XRL beam was also characterised in terms of optical parameters such as divergence, spatial coherence and polarisation. The divergence of the seeded XRL was slightly lower than those of the seed. The brightest part of the image in Fig. 4 corresponds to the seeded XRL while the weak surrounding, circular signal is the ASE x-ray laser. The divergence of the ASE x-ray laser was found to be much larger (>12 mrad) than that of the seeded beam (1 mrad). Moreover, no sign of depolarisation has been observed.

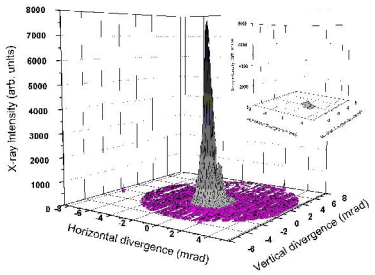

Figure 3 : 3D images (false color) of the seeded XRL cross-section as recorded by the XUV CCD detector

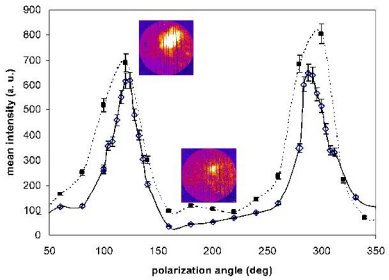

Figure 4 : Variation of the HHG (open diamond) and seeded XRL (black square) intensities versus the angle of polarization.

By comparing the images in Fig. 6, one may estimate the ratio between the seeded XRL and the ASE total energies. When the seed was heavily saturated, the energy contained in the seeded XRL was about 17 times higher than the energy of the ASE XRL. Note that the ASE level might be easily reduced to a negligible level by placing an aperture selecting only the seeded beam. Knowing the ASE level, we estimated the seeded XRL photon number to be about 10^{11} per pulse (~0.7 μJ). On all the images of seeded XRL cross-section, strong diffraction structures appeared close to alignment wires. For HHG and seeded XRL the diffraction was highly contrasted showing that the seeded XRL kept the high degree of coherence of the HHG. ASE x-ray laser alone generated hardly visible diffraction fringes confirming the expected weak coherence. From previous measurements of the ASE XRL wave front[8] we may expect to maintain the seeded XRL as good as the HHG wave front.

REFERENCES

[1] Ph. Zeitoun. et al. , A high-intensity highly coherent soft X-ray femtosecond laser seeded by a high harmonic beam, Nature vol 431, 426-429 (2004)

*[2] Kazamias, S. et al, Global optimization of High Harmonic generation. Phys. Rev. Lett., **90**, 193901 (2003)*

*[3] Lemoff, B.E., Barty, C.P.J. and Harris, S.E., Femtosecond-pulse-driven, electron-excited XUV lasers in eight-times-ionized noble gases. Opt. Lett., **19**, 8, 569 (1994)*

*[4] Sebban, S. et al, Saturated Amplification of a Collisionally Pumped Optical-Field-Ionization Soft X-Ray Laser at 41.8 nm. Phys. Rev. Lett. **86**, 3004 (2001).*

*[5] Sebban, S., Demonstration of a Ni-Like Kr Optical-Field-Ionization at 32.8 nm. Phys. Rev. Lett., **89**, 253901 (2002).*

Frontiers of molecular science based on molecular manipulation techniques

Hirofumi Sakai
Department of Physics, Graduate School of Science, The University of Tokyo
7-3-1, Hongo, Bunkyo-ku, Tokyo 113-0033, Japan
hsakai@phys.s.u-tokyo.ac.jp

A sample of aligned or oriented molecules is an ideal quantum system to investigate the quantum phenomena associated with the correlation between the molecular axis and the (time-dependent) polarization pulses and with molecular symmetries. Therefore, it is quite natural that controlling external degrees of freedom of molecules has been one of very active research areas in physics and chemistry in recent years. Our clear demonstration of one-dimensional molecular alignment [1,2] is followed by a series of demonstrations of three-dimensional alignment [3], one-dimensional orientation [4,5], and recent three-dimensional orientation [6]. In my talk, I will present two illustrative experiments pointing to new directions in molecular science experiments with a sample of aligned molecules.

The first demonstration has been performed with a sample of *adiabatically* aligned I_2 molecules. We have succeeded in controlling multiphoton ionization processes with time-dependent polarization pulses, which are introduced as a new control parameter [7,8]. Much better controllability is achieved with a time-dependent polarization pulse than with a pulse having a fixed ellipticity. The results suggest the existence of an unknown tunnel ionization mechanism which is characteristic of a time-dependent polarization pulse and have triggered theoretical studies [9].

This demonstration points to new directions in optimal control studies with molecular systems: (1) A sample of aligned molecules is used in the optimal control experiment for the first time. (2) In order to optimize the quantum processes in molecules, time-dependent polarization pulses are applied to the learning-loop optimal control system for the first time. The importance of time-dependent polarization pulses has been discussed in Ref. [10]. (3) Using a sample of aligned molecules and a time-dependent polarization pulse, both external and internal degrees of freedom in molecules are simultaneously controlled.

The second demonstration has been performed with a sample of *nonadiabatically* aligned molecules. We report the first demonstration of quantum interference of electron de Broglie waves evidenced by high-order harmonic generation from aligned CO_2 molecules [11]. The quantum interference is the highlight phenomenon expected to be observed in aligned molecules. The observation of the quantum interference has been made possible by the simultaneous observation of ion yields and high-order harmonics under the same experimental conditions. This experimental technique can serve to disentangle the contributions from the ionization and recombination processes. In order to explain the observed quantum interference, we successfully extend a model of two point emitters, which was originally proposed to a diatomic molecule [12], to a triatomic molecule.

Based on the fact that the interference takes place within one optical cycle, we propose a new route to image the instantaneous structure of molecular systems [11]. The procedures of this new imaging technique are as follows. (1) Prepare a sample of highly aligned molecules. (2) Observe the angular dependence of ion yields ($I_{\mathrm{ion}}(\theta)$)

and harmonic signals ($I_{HH}(\theta)$) of an appropriate harmonic order (for which destructive interference can be expected) from aligned molecules by rotating the polarization direction of the probe pulse. Here, the orientation angle θ is the angle between the molecular axis and the polarization direction of the probe pulses. (3) Plot a graph of the ratio $I_{HH}(\theta)/I_{ion}(\theta)$ against θ, which should give the angular dependence of the recombination probability $I_{recom}(\theta)$ (Remember that $I_{HH}(\theta) \sim I_{ion}(\theta) \times I_{recom}(\theta)$). (4) Find the angle θ at which a dip appears in the graph. (5) Then the instantaneous bond length R can be determined by the condition for destructive interference. The resolution of the measurement could be less than one optical cycle if we employ few-cycle pulses as probe pulses. This new approach to probe the instantaneous structure of molecular systems has also been discussed in Ref. [13].

[1] H. Sakai, C. P. Safvan, J. J. Larsen, K. M. Hilligsøe, K. Hald, and H. Stapelfeldt, J. Chem. Phys. **110**, 10235 (1999).
[2] J. J. Larsen, H. Sakai, C. P. Safvan, I. Wendt-Larsen, and H. Stapelfeldt, J. Chem. Phys. **111**, 7774 (1999).
[3] J. J. Larsen, K. Hald, N. Bjerre, H. Stapelfeldt, and T. Seideman, Phys. Rev. Lett. **85**, 2470 (2000).
[4] H. Sakai, S. Minemoto, H. Nanjo, H. Tanji, and T. Suzuki, Phys. Rev. Lett. **90**, 083001 (2003).
[5] S. Minemoto, H. Nanjo, H. Tanji, T. Suzuki, and H. Sakai, J. Chem. Phys. **118**, 4052 (2003).
[6] H. Tanji, S. Minemoto, and H. Sakai, submitted.
[7] T. Suzuki, S. Minemoto, T. Kanai, and H. Sakai, Phys. Rev. Lett. **92**, 133005 (2004).
[8] T. Suzuki, S. Minemoto, and H. Sakai, Appl. Opt. **43**, 6047 (2004).
[9] T. Kanai, S. Minemoto, and H. Sakai, Ultrafast Phenomena XIV, T. Kobayashi *et al*. (Eds.) Springer, pp. 310-312 (2005).
[10] Y. Silberberg, Nature (London) **430**, 624 (2004).
[11] T. Kanai, S. Minemoto, and H. Sakai, Nature (London) **435**, 470 (2005).
[12] M. Lein, N. Hay, R. Velotta, J. P. Marangos, and P. L. Knight, Phys. Rev. Lett. **88**, 183903 (2002).
[13] J. P. Marangos, Nature (London) **435**, 435 (2005).

Observation of the Wave Packet Dynamics by femtosecond luminescence spectroscopy

Tohru Suemoto
Institute for Solid State Physics, The University of Tokyo, 5-1-5 Kashiwanoha, Kashiwa-shi, Chiba, 277-8581, Japan

The motion of atoms in molecules or solids can be viewed as a dynamics of the nuclear wave-packet propagating on adiabatic potential surfaces. The wave-packet oscillations in free molecules have been extensively studied by A. H. Zewail and other groups. However, in most of the cases, the shape of the wave-packet has not been captured, because the oscillation has been observed in a very restricted region on the potential surface and the quantitative information of the position on the potential surface has not been obtained. On the other hand, the luminescence methods we employed can resolve these difficulties inherent to the transient absorption methods. In this presentation I will review the recent achievements in our group.

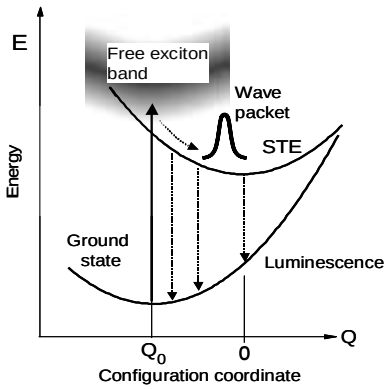

Fig. 1 Adiabatic potential curves for self-trapped excitons

We succeeded in making a movie of the wave-packet for the self-trapped exciton in a quasi-one-dimensional halogen-bridged platinum complex (abbreviated as Pt-Br). In this material, the excitons created by light excitation immediately localizes accompanying a large lattice distortion and the local vibration mode is excited during this localization process. As shown in Fig. 1, the emission energy from the lowest excited state depends on the position of the wave-packet. Therefore, the time-resolved luminescence spectrum directly reflects the position and the shape of the wave-packet. We excited the sample by 25 fs pulses from a mode-locked Ti-sapphire laser and measured the time-development of the luminescence intensity by using a sum frequency gating (up-conversion) method. Figure 2 shows the time-dependent luminescence spectra in a gray scale plot on time-energy axes (room temperature). Figure 3 shows several frames of the time-resolved spectra, i.e. the snapshots of the wave-packet deduced from Fig. 2 and compared with calculated results for a harmonic oscillator. We can clearly see good agreements in the features such as the peaking and the asymmetry of the wave at the turning points [1].

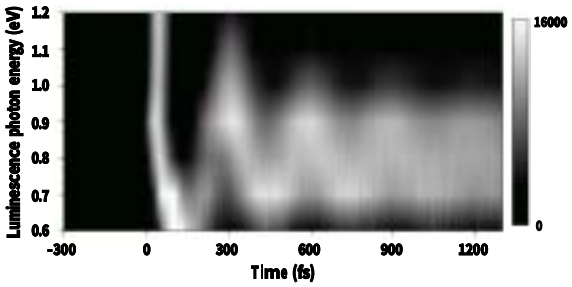

Fig. 2 Gray scale plot of the wave-packet in Pt-Br.

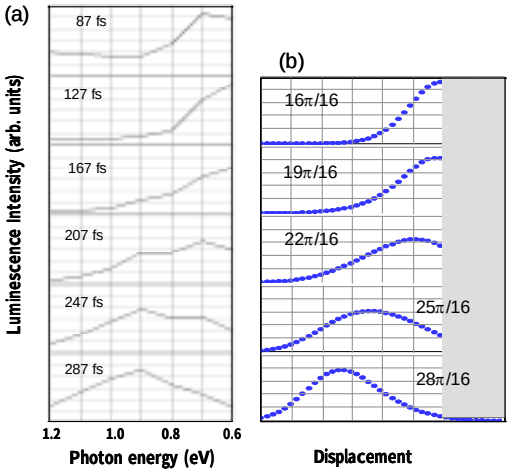

Fig. 3 Snapshots of the wave-packets in experiment (a) and calculation (b) for Pt-Br.

In the same material at a low temperature (4K), we observed complicated oscillation patters as shown in Fig. 4. At 0.95 eV, the fundamental oscillation at 3.3 THz seems to be modulated by a

lower frequency. At 0.85 eV, the oscillation persists rather long and disappears suddenly around 3 ps. From a Fourier transform of the waveform, we found a new oscillating component at 0.7 THz. However, it is impossible to reproduce such complicated waveforms by simply superposing the two damped sinusoidal waves. In order to understand these waveforms, we assumed a two dimensional motion of the wave-packet on an adiabatic potential surface corresponding to these two frequencies. As is well known, the motion of the mass point on such a potential will produce a Lissajous figure. By assuming an appropriate parameters including damping constants, we reproduced the waveform as shown by thin black lines in Fig. 4 [2].

Another family of systems we studied are the F-centers in alkali-halides. The F-center is a halogen ion vacancy with a trapped electron and roughly viewed as a hydrogen atom embedded in a dielectrics. After excitation of the system from the 1s ground state to the 2p state, we observed an oscillating signal of the luminescence as shown in Fig. 5. The peculiar point in this observation is the existence of the very fast rising component of the luminescence intensity near the potential minimum. Normally, the population of the system at the potential minimum rises slowly in a time corresponding to several oscillation periods. Therefore, this fast rise (order of 1/4 period) cannot be understood in terms of damped harmonic oscillator. This suggest demolition of the wave-packet due to a fast decoherence process. The tunneling from the 2s-like state to the closely located 2p-like state can be the origin of such a process [3].

In the F-centers in KBr, the dynamics of the wave-packet in the excited state was experimentally separated from the wave-packet dynamics [4] in the ground state, which can be assigned to the hole oscillation [5].

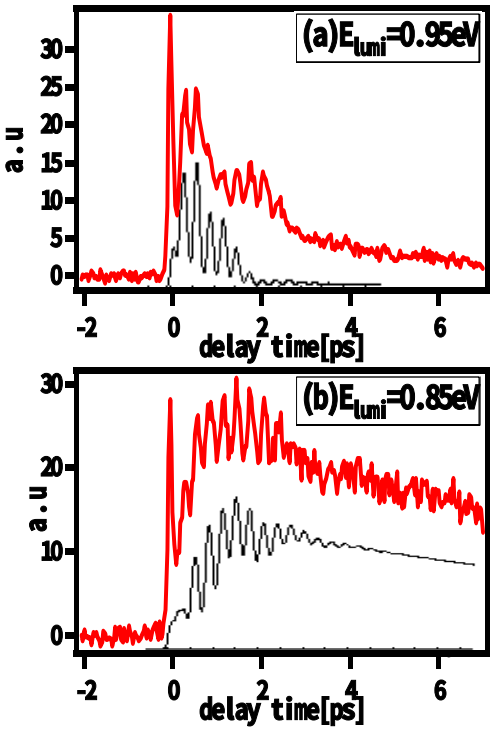

Fig. 4 Time-evolution of the luminescence intensity in Pt-Br at 4K. Gray and black curves correspond to experiment and calculation, respectively.

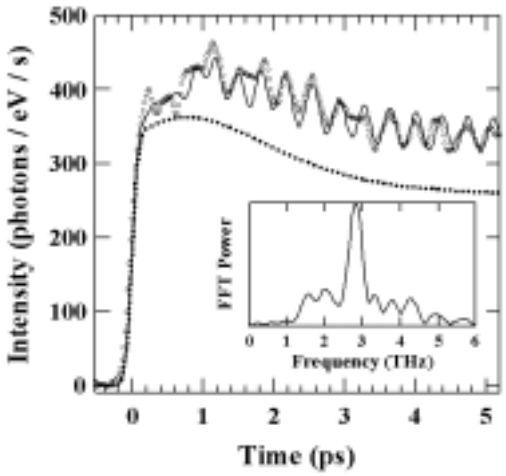

Fig. 5 Time-evolution of the luminescence intensity in KI:F-center at 0.9 eV. Dotted line shows the incoherent component. The inset is the Fourier power spectrum.

[1] T. Matsuoka et al., Phys. Rev. Lett. 91, 247402 (2003)
[2] K. Yasukawa et al., Technical Digest of IQEC(Tokyo, 2005)
[3] T. Koyama et al., Technical Digest of IQEC (Tokyo, 2005)
[4] M. Nisoli et al., Phys. Rev. Lett. 84, 4425 (1996)
[5] Y. Kayanuma and S. Tanaka, Pys. Rev. B62, 12838 (2000)

Photoluminescence and lasing in highly uniform T-shaped quantum wires

Masahiro Yoshita
Institute for Solid State Physics, University of Tokyo and CREST, JST,
5-1-5 Kashiwanoha, Kashiwa, Chiba 277-8581, Japan
E-mail: yoshita@issp.u-tokyo.ac.jp

High quality T-shaped quantum wire (T-wire) lasers were fabricated by the cleaved-edge overgrowth method with molecular beam epitaxy. A single T-wire laser structure fabricated is shown in Fig. 1. The quantum-wire states are formed at a right-angled T-shaped intersection of two quantum wells; (001) quantum well (stem well) and (110) quantum well (arm well). To improve interface quality of the T wire, we performed high-temperature growth-interruption annealing on the (110) growth surface of the arm well [1].

Micro-photoluminescence (PL) and PL excitation (PLE) spectroscopy reveals unprecedented high quality of the wires. PL peaks from the wire show a narrow linewidth of about 1 meV, and both the intensity and energy position of the peaks are spatially uniform over 20 μm. In PLE spectra, distinct structures of one-dimensional (1D) free excitons and 1D continuum states are observed [2]. Waveguide transmission spectroscopy has revealed that the 1D exciton ground state for the single T wire has a large absorption coefficient of 80 cm^{-1} at 5 K [3].

We achieved ground state lasing in single-quantum-wire lasers (T < 60K) [4], which is shown in Fig. 2, as well as 20-quantum-wire lasers (T < 120K) [5] by optical pumping. The wires tend to lase in a single mode at energy with a relatively small shift. Lasing threshold of T wires was lower than that of quantum wells formed in the same samples. Near field pattern of the T-wire laser shows a very good circular shape [6].

Gain mechanism of the quantum-wire lasers is argued in comparison with PL and gain measurements. Figure 3 shows PL spectra of the single T wire for various excitation powers or electron-hole densities. The PL spectra evolve from a sharp free exciton peak to a red-shifted PL band with symmetric broadening as the excitation level is increased [7]. The lasing energy (1.577eV) is about 5 meV below the free exciton, and is on the red-shifted broad PL band. The evolution of this PL band suggests formation of an electron-hole plasma with strong Coulomb interactions [5,7].

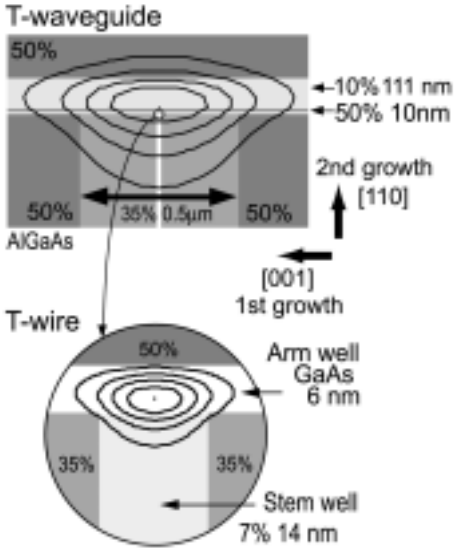

Fig. 1. Schematic of a single T-wire laser structure. Percentages show Al contents (x) in $Al_xGa_{1-x}As$ layers

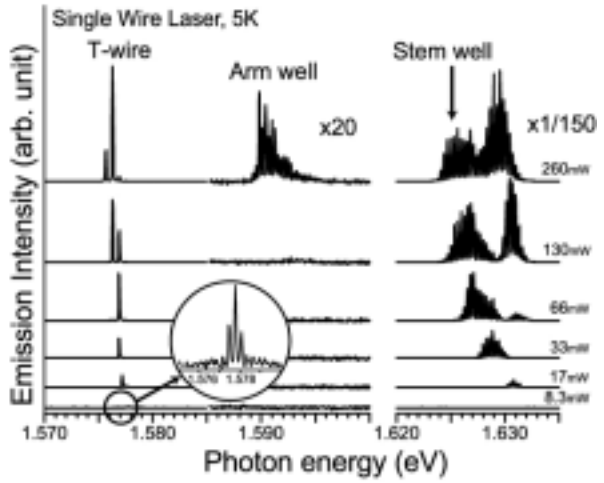

Fig. 2. Stimulated emission spectra of the single T-wire laser at 5 K for various optical pumping powers.

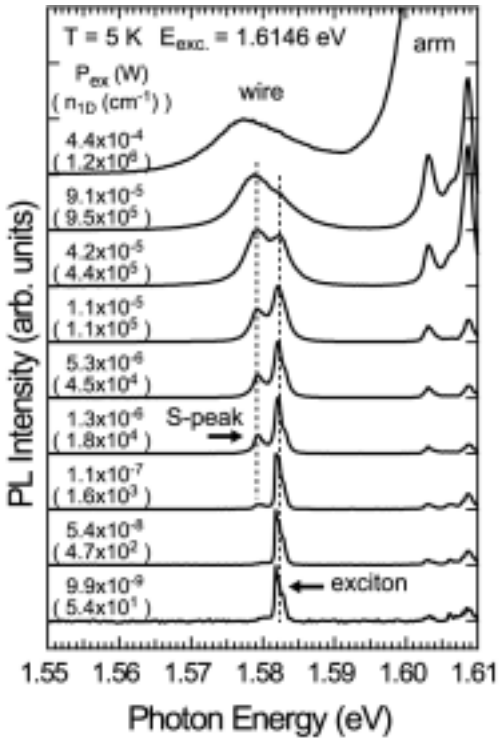

Fig. 3. Normalized PL spectra of the T wire for various excitation powers (P_{ex}) at 5 K. Estimated 1D e-h pair densities are indicated in parentheses.

Recent measurements of gain spectra via the Cassidy's method (a modified method of the Hakki-Paoli method) strongly support this assignment [8]. It is concluded that the origin of lasing is the 1D electron-hole plasma with strong Coulomb interactions.

[1] M. Yoshita et al., JJAP **40**, L252 (2001); APL **81**, 49 (2002); J. W. Oh et al., APL **82**, 1709 (2003). [2] H. Itoh et al., APL **83**, 2043 (2003); H. Akiyama et al., APL **82**, 379 (2003). [3] Y. Takahashi et al., **86**, 243101 (2005). [4] Y. Hayamizu et al., APL **81**, 4937 (2002). [5] H. Akiyama et al., PRB **67**, 041302(R) (2003). [6] Y. Takahashi et al., APL **83**, 4089 (2003). [7] M. Yoshita et al., cond-mat/0402526. [8] Y. Hayamizu et al., ICPS2004.

Recent Progress in Liquid Crystal THz Optics

Ci-Ling Pan
Department of Photonics and Institute of Electro-Optical Engineering
National Chiao Tung University
Hsinchu, Taiwan 30010, ROC

Abstract

In the past decade, THz studies ranging from investigations of ultrafast dynamics in materials to medical, environmental sensing and imaging have been actively explored. For these and future applications in THz communication and surveillance, quasi-optic components such as phase shifters are indispensable. The birefringence of liquid crystals (LC's) is well known and extensively utilized for the manipulation of optical radiation in the visible and near-infrared range. Recently, there have been increasing interests in the study of liquid-crystal-based devices for application in the sub-millimeter wave or THz frequency range. In this talk, we present recent progress in liquid crystal THz optics from our group. Using time-domain THz spectroscopy, we have determined the complex indices of refraction of a nematic liquid crystal, 5CB, PCH5 and E7 from 0.2 to beyond 1 THz. Significantly, the birefringence of 5CB and E7 are found to be as large as 0.2 at THz frequencies, while the absorption is negligible [1-3]. Electrical-field and magnetic-field-controlled birefringence in LC were also reported [4-6]. A tunable room-temperature THz phase shifter using magnetic-field-controlled birefringence in nematic 5CB gives a phase shift as large as 108° at 1.0 THz [5]. Phase shift exceeding 360° at 1 THz, an important milestone, was realized by using a sandwiched LC (E7, Merck) cell as thick as 3 mm [6]. Finally, we will present initial works on control of enhanced THz transmission through a metallic hole array with nematic liquid crystals [7]. Our work clearly demonstrates the device potential of liquid crystal devices.

1. Tsong-Ru Tsai, Chao-Yuan Chen, Ci-Ling Pan, Ru-Pin Pan, and X.-C. Zhang, "THz Time-Domain Spectroscopy Studies of the Optical Constants of the Nematic Liquid Crystal 5CB", Appl. Optics, Vol. 42, No. 13, pp 2372-2376 (May 1, 2003) .
2. Ru-Pin Pan, Tsong-Ru Tsai, Chao-Yuan Chen, and Ci-Ling Pan, "Optical Constants of Two Typical Liquid Crystals 5CB and PCH5 in the THz Frequency Range", J. of Biological Physics, V. 29, No.2-3, pp.335-338, July, 2003.
3. Ru-Pin Pan, Tsong-Ru Tsai, Chiunghan Wang, Chao-Yuan Chen, And Ci-Ling Pan, "The Refractive Indices of Nematic Liquid Crystal 4, 4'-n-pentylcyanobiphenyl in the THz Frequency Range," Mol. Cryst. Liq. Crystl., Vol. 409, pp. 137-144, 2004.
4. Tsong-Ru Tsai, Chao-Yuan Chen, Ci-Ling Pan, Ru-Pin Pan, and X.-C. Zhang, "Room Temperature Electrically Controlled Terahertz Phase Shifter," IEEE Microwave and Wireless Components Lett., Vol. 14, No. 2, pp. 77-79, February 2004.
5. Chao-Yuan Chen, Tsong-Ru Tsai, Ci-Ling Pan, and Ru-Pin Pan"Terahertz Phase Shifter with Nematic Liquid Crystal in a Magnetic Field", Appl. Phy. Letts, Vol.83, no.22, pp4497-4499, December 1, 2003.
6. Chao-Yuan Chen, Cho-Fan Hsieh, Yea-Feng Lin, Ru-Pin Pan, and Ci-Ling Pan, "Magnetically Tunable Room-Temperature 2π Liquid Crystal Terahertz Phase Shifter," Opt. Express, Vol. 12, No. 12, pp. 2625-2630 June 14, 2004.
7. Ci-Ling Pan, Cho-Fan Hsieh, and Ru-Pin Pan, Masaki Tanaka, Fumiaki Miyamaru, Masahiko Tani, and Masanori Hangyo, "Control of enhanced THz transmission through metallic hole arrays using nematic liquid crystal," Optics Express, Vol. 13, No. 11, pp. 3921 - 3930, May 30, 2005.

Terahertz Hall measurements by magneto-optical spectroscopy

Ryo Shimano
Department of Physics, School of Science,
University of Tokyo, 7-3-1Hongo, Bunkyo-ku, Tokyo, 113-0033, Japan

Magneto-optical effect such as Faraday effect or magneto-optical Kerr effect (MOKE) has been powerfully used to investigate the ultrafast spin dynamics and transport properties in solid states under magnetic field, by optical means. With recent advances in THz technology, it has become possible to perform the magneto-optical measurements even in THz frequency region. Since the electromagnetic responses of materials in THz frequency region are sensitive to the motion of free carriers, THz Faraday effect or MOKE is equivalent to the high frequency ac Hall effect.

The spectral response of ac Hall effect provides us deep insights into the dynamical properties of scattering processes of electrons under magnetic field or magnetization. In particular, the ac Hall response has been extensively investigated in those exotic materials such as superconductors. A discrepancy from simple Drude model has been reported. The frequency dependence of ac Hall effect has been discussed in connection with the anomalous temperature dependence of normal state dc Hall effect in cuprate superconductors.

The spectrum of Hall angle $\cot\Theta=\sigma_{xx}/\sigma_{xy}$ is experimentally obtained through the measurement of magneto-optical signal, i.e., the polarizarion rotation and ellipticity of transmitted or reflected light. The rotation angle in such materials is typically very small, of the order of mrad in THz frequency region even under relatively high magnetic field of several Tesla. Accordingly, a high sensitive polarization detection scheme is required.

To this end, we have been developing magneto-optical polarization spectroscopy based on THz-TDS. In this talk, I will present our recent progress on the development of THz polarimeter with sensitivity of sub-mrad. I will also present on the development of frequency tunable THz circular polarization control scheme, which can be applied to THz circular dichroism measurements. This work has been done in collaboration with Y. Ino, H. Nishimura, and M. Gonokami.

References

[1] R. Shimano, Y. Ino, Yu. P. Svirko, and M. Kuwata-Gonokami, ”Terahertz frequency Hall measurement by magneto-optical Kerr spectroscopy in InAs”, Appl. Phys. Lett. **81**, 199 (2002).
[2] Y. Ino, R. Shimano, Yu. P. Svirko, and M. Kuwata-Gonokami, “Terahertz time domain magneto-optical ellipsometry in reflection geometry”, Phys. Rev. B, **70**, 155101(2004).
[3] R. Shimano, H. Nishimura, and T. Sato, “Frequency Tunable Circular Polarization Control of Terahertz Radiation”, Jpn. J. Appl. Phys. **44**, L676 (2005).

Email address: shimano@phys.s.u-tokyo.ac.jp

Optical Manipulations for Testing Macromolecular Interactions and New Ideas in Statistical Mechanics

Masaki Sano, Yoshihiro Murayama, Hong-ren Jiang, and Shoichi Toyabe
Department of Physics, The University of Tokyo, 3-7-4 Hongo, Bunkyo-ku, Tokyo, 113-0033, Japan

Optical forces produced by strongly focused laser beam are suitable to manipulate objects ranging from tens of nanometers to tens of micrometers. Thus the optical trap, so-called optical tweezers, has become an important tool for research in the fields of physical, chemical, and biological sciences. In fact many interesting problems in biology and soft matter physics are accessible by using optical tweezers in the view point of length scale and time scale. One of the examples is to study interaction of macromolecules such as DNA, RNA, actin filaments, etc. Other example can be found in mesoscopic systems where thermal fluctuations paly an important role. Recent technical progress in optical manipulations offers possibility to test new ideas in statistical mechanics in mesoscopic systems. We will present two topics from these aspects.

1. Phase Transition of Single DNA molecules

Higher order structures of DNA and structural transitions are studied with focusing on the interactions between DNA and several macro-ions in water solutions by using single molecular measurement technique. We measured elastic response of single DNA molecules at various concentrations of trivalent cation, spermidine using laser tweezers. When added spermidine caused the DNA to collapse, the force-extensiton curves showed either plateaus or stick-release patterns depending on the concentration. The periodic stick-release response determines a characteristic length, which may reflect toroidal supercoiling of DNA molecules. At high concentrations of spermidine, we observed the reelongation of single molecules of collapsed DNA. Thus reentrant occurs between lower and upper critical concentrations, verifying that the transition is reentrant as theoretically predicted. Furthermore, by measuring

2. Testing New Ideas in Statistical Mechanics

Brownian motions of colloidal particles are well understood in the framework of fluctuation-response theorems. However, when the particles are driven to far from equilibrium, only little is known about quantitative relations among physical measures. Very recently, some new ideas in statistical mechanics, such as the fluctuation theorem, Jarzynski equation, and Harada-Sasa's relation, are proposed. These new ideas formulate quantitative relations among fluctuations, dissipation, and entropy production in systems far from equilibrium. Multiple and multifunctional optical traps can be used to create prescribed potential fields and time dependent forces exerted on Brownian particle and become useful tools to test new relations in statistical mechanics.

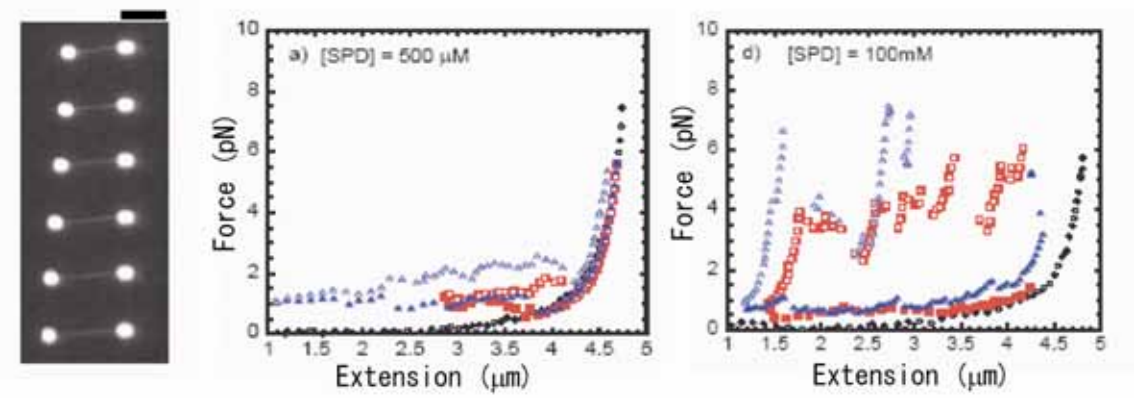

Fig.1 (left): Visualization of stretched DNA, (middle, right): Force extension curves of DNA

The Allosteric Transition of the Chaperonin GroEL Studied by Solution X-ray Scattering and Fluorescence Spectroscopy

Kunihiro Kuwajima
Department of Physics, Graduate School of Science, University of Tokyo, 7-3-1 Hongo, Bunkyo-ku, Tokyo 113-0033, Japan
E-mail: *kuwajima@phys.s.u-tokyo.ac.jp*

The chaperonin GroEL from *Escherichia coli* is a tetradecameric protein complex of 14 identical 57 kDa subunits arranged in two heptameric rings stacked back-to-back with a central cavity. This protein is known to undergo cooperative allosteric transitions induced by ATP, and these allosteric transitions must be important for functional activities of the chaperonin as a molecular chaperone. We have recently studied the allosteric transitions of GroEL induced by ATP and a series of metal fluoride-ADP complexes using small angle X-ray scattering and fluorescence spectroscopy in combination with a stopped-flow technique.

An important issue on the ATP-induced allosteric transition of GroEL is identification of the allosteric conformational transition in complex kinetics of GroEL observed by fluorescence and other spectroscopic techniques. With X-ray scattering one can clearly distinguish the three allosteric states of GroEL, and the kinetics of the transition of GroEL induced by 85 μM ATP have been observed directly by stopped-flow X-ray scattering. The rate constant has been found to be 3-5 s^{-1} at 5°C, indicating that this process corresponds to the second phase of the ATP-induced kinetics of tryptophan-inserted GroEL measured by stopped-flow fluorescence. The ATP-induced fluorescence kinetics (the first and second phases) at various ATP concentrations (< 400 μM) occur before ATP hydrolysis by GroEL takes place and are well explained by a kinetic allosteric model, which is a combination of the conventional transition state theory and the Monod-Wyman-Changeux allosteric model.

Another important issue on the allosteric transition of GroEL is its strikingly high specificity for ATP as an effective allosteric ligand. Among ATP, ADP, and other adenine nucleotides, including ATP-γS and AMP-PNP, only ATP can induce the allosteric transition. To understand the mechanism of the allosteric transition, we have studied the effect of a series of metal fluoride ADP complexes and vanadate-ADP on GroEL by kinetic fluorescence measurement of pyrene-labeled GroEL and by small-angle X-ray scattering measurement of wild-type GroEL. The metal fluorides and vanadate, complexed with ADP, are known to mimic the γ-phosphate group of ATP, but they differ in geometry and size. Therefore, it is expected that these compounds will be useful for investigating the high specificity of GroEL for ATP that enables the induction of the allosteric transition. The kinetic fluorescence measurement revealed that aluminium, beryllium, and gallium ions, when complexed with the fluoride ion and ADP, induced a biphasic fluorescence change of pyrenyl-GroEL, while scandium and vanadate ions did not induce any kinetically observed change in fluorescence.

The X-ray scattering measurements indicated that the allosteric state induced by these metal fluoride-ADP complexes is structurally equivalent to the allosteric state induced by ATP. It is concluded that the tetrahedral geometry of γ-phosphate (or its analogs) and the inter-atomic distance (~1.6 Å) between phosphorous (vanadium, or metal atom) and oxygen (or fluorine) are both important for inducing the allosteric transition of GroEL, leading to the high selectivity of GroEL for ATP about ligand adenine nucleotides, which function as the preferred allosteric ligand.

Both of the above studies thus clearly indicate that the solution X-ray scattering is extremely powerful for investigating the equilibrium and kinetics of cooperative conformational transitions of oligomeric protein complexes, especially when combined with other spectroscopic techniques such as fluorescence spectroscopy.

REFERENCES

1. Inobe, T., Arai, M., Nakao, M., Ito, K., Kamagata, K., Makio, T., Amemiya, Y., Kihara, H. & Kuwajima, K. (2003). Equilibrium and kinetics of the allosteric transition of GroEL studied by solution X-ray scattering and fluorescence spectroscopy. *J Mol Biol* **327**, 183-191.
2. Inobe, T., Kikushima, K., Makio, T., Arai, M. & Kuwajima, K. (2003). The allosteric transition of GroEL induced by metal fluoride-ADP complexes. *J Mol Biol* **329**, 121-134.
3. Inobe, T. & Kuwajima, K. (2004). Phi value analysis of an allosteric transition of GroEL based on a single-pathway model. *J Mol Biol* **339**, 199-205.